Journal of Hazardous Materials 211–212 (2012) 296–303

Contents lists available at SciVerse ScienceDirect

Journal of Hazardous Materials

journal homepage: www.elsevier.com/locate/jhazmat

Efficient desulfurization by polymer–inorganic nanocomposite membranes fabricated in reverse microemulsion

Ben Li[a,b], Shengnan Yu[a,b], Zhongyi Jiang[a,b,*], Wanpeng Liu[a,b], Ruijian Cao[a,b], Hong Wu[a,b]

[a] Key Laboratory for Green Chemical Technology, Ministry of Education of China, School of Chemical Engineering and Technology, Tianjin University, Tianjin 300072, PR China
[b] State Key Laboratory of Materials-Oriented Chemical Engineering of Nanjing University of Technology, Nanjing 210009, PR China

ARTICLE INFO

Article history:
Received 13 May 2011
Received in revised form 9 October 2011
Accepted 14 October 2011
Available online 20 October 2011

Keywords:
Gasoline desulfurization
Nanocomposite membrane
Biomimetic mineralization
Reverse microemulsion
Pervaporation

ABSTRACT

The sulfur in gasoline will convert to SO_2 after combustion under high temperature, which adversely affects human health and the environment. Membrane technique in particular pervaporation offers a number of potential advantages over conventional FCC gasoline desulfurization processes. The present study focuses on the performance enhancement of PDMS membrane by incorporating silica nanoparticles. Specifically, silica nanoparticles formed by the catalysis and templating of protamine in w/o reverse microemulsion are in situ embedded into PDMS bulk matrix, endowing the resultant oleophilic nanocomposite membranes with appropriate free volume properties and superior separation performance. Through the rational manipulation of biomimetic mineralization at water–oil interface, silica particles with uniform size are acquired. Following this protocol, by introducing organic PDMS oligomers into the oil phase, PDMS–SiO_2 nanocomposite membranes are prepared in a facile way. The resultant nanocomposite membranes display superior permeability and permselectivity in the pervaporative desulfurization using thiophene/*n*-octane binary mixture as model gasoline, for example, under the condition of 500 ppm sulfur in feed (40 L/h) at 30 °C, an enrichment factor of 4.83–5.82 with a normalized permeation rate of 6.61–10.76 × 10^{-5} kg m/m^2 h is acquired.

1. Introduction

Sulfur in gasoline reduces the activity of vehicle catalytic converters by poisoning the active sites, thus increasing exhaust gases from motor vehicles that adversely affect human health and the environment [1,2]. This obliges numerous countries to adopt new regulations, aiming at a notable reduction of sulfur emissions by imposing a very low concentration of sulfur in fuels. The European Union stipulates that the limitation of sulfur in gasoline should be minimized to 10 ppm since 2009 [3]. The California Reformulated Gasoline Regulations (CaRFG) requires the content cap limits of 20 ppm from the end of the year 2011 [4]. Legislations in China have been established to reduce the sulfur content in gasoline to 150 ppm since 2010, and the capital city Beijing has executed a standard of 50 ppm from 2008 [5].

Hydrodesulfurization (HDS) process constitutes the most effective method, presently [6]. However, the HDS suffers from the high cost of hydrogen and the notable decrease of octane number of gasoline after treatment. Compared with traditional HDS method, membrane technique offers a number of potential advantages, including higher selectivity, lower operating and energy costs, facile scale-up, and large flexibility for future regulatory compliance. It would be thus highly desirable to develop a selective membrane separation technique in particular pervaporation for the deep reduction of sulfur in hydrocarbon streams [7].

Polydimethylsiloxane (PDMS) as an important membrane material is widely used in the desulfurization of gasoline by pervaporation. However, pure PDMS membrane often suffers from low selectivity and poor mechanical strength. Introducing inorganic components to acquire hybrid or nanocomposite membranes in many cases could markedly improve the properties of the membrane. The intermolecular interactions and energy dissipation between inorganic and organic moieties endow the nanocomposite membranes with complementary and unique macroscopic properties [8–11]. Up to now, the common strategies for fabricating nanocomposite membranes include physical blending and sol–gel soft chemistry, which suffer from some inherent drawbacks [12,13]. If we turn our eyes to nature, most cell walls, actually, are comprised of polymer–inorganic nanocomposite materials [14]. Biomineralization using intricate biomacromolecules, e.g., peptides, proteins/enzymes, polysaccharides, and viruses have

* Corresponding author at: Key Laboratory for Green Chemical Technology, Ministry of Education of China, School of Chemical Engineering and Technology, Tianjin University, Tianjin 300072, PR China. Tel.: +86 22 23500086; fax: +86 22 23500086.
E-mail address: zhyjiang@tju.edu.cn (Z. Jiang).

0304-3894/$ – see front matter © 2011 Elsevier B.V. All rights reserved.
doi:10.1016/j.jhazmat.2011.10.047

depicted the power for catalyzing and structurally directing inorganic precursors into inorganic minerals [15–18]. Compared to conventional chemical synthesis that often requires critical conditions, bio-inspired method often proceeds under much milder conditions (aqueous solution, neutral or near neutral pH, and ambient temperature). Moreover, bio-inspired silica synthesis imposes much more delicate control over the hierarchical architectures (size, shape, morphology, and pore structure) of silica nanoparticles. Not surprisingly, biomineralization paves the prospective way for the fabrication of organic–inorganic nanocomposite membranes with elaborate geometries under very mild conditions.

In most cases, biomineralization necessitates aqueous environment. As a consequence, research efforts are overwhelmingly devoted to biomineralization in aqueous phase and related to silica, calcium carbonate, hydroxyapatite, as well as hydrophilic polymer–inorganic nanocomposite membranes [19,20]. Rare reports, however, are related to the straightforward synthesis of the oleophilic polymer based nanocomposite membranes through biomimetic mineralization. Oleophilic polymer is usually dissolved in a nonaqueous oil-based solvent; it is thus quite difficult to simultaneously manipulate the hydrolysis–condensation of inorganic precursors and cross-linking of oleophilic oligomers in a homogenous phase. Therefore, it could be envisaged that one-step fabrication of oleophilic polymer membranes embedded with uniformly distributed inorganic components will bear both academic and technological significance.

Inspired by the silica formation process mediated by silica deposition vesicle (SDV) [21,22], in the current study, oleophilic nanocomposite membranes are fabricated by manipulating the in situ biomineralization within the underlying equilibrated and thermodynamically stable water-in-oil (w/o) reverse microemulsions. The confined space endows biocompatible environment for biomacromolecules, which consequently direct inorganic precursors polymerization through interfacial molecular recognition and subsequent hydrolysis–condensation reactions [23]. In the current study, PDMS–SiO_2 nanocomposite membranes are in situ prepared through the polymerization of PDMS oligomers in the oil phase and silica precipitation in the reverse microemulsion simultaneously. It should be noted that the introduction of PDMS should enhance the preparation process stability, because it increases the viscosity of the reverse microemulsion, reducing the probability of collision between the droplets [24]. The structural morphology, mechanical strength, crystallinity, and free volume characteristics of the PDMS–SiO_2 nanocomposite membranes were systematically investigated. Using the mixture of *n*-octane/thiophene as the model gasoline system, the pervaporative desulfurization properties were systematically evaluated.

2. Experimental

2.1. Materials

Protamine sulfate salt, tris (hydroxymethyl) amino methane hydrochloride (Tris–HCl), tetraethyl orthosilicate (TEOS) were purchased from Sigma–Aldrich. Tween 80, Span 80, *n*-heptane, *n*-octane and thiophene were supplied by GuangFu fine chemical research institute, China. PDMS oligomer (the viscosity was 5000 mPa s, and the corresponding average molecular weight was about 40,000), dibutyltin dilaurate were obtained from Beijing Chemical Company, China. Asymmetric polysulfone (PS) ultrafiltration membranes were ordered from Shanghai Mega Vision Membrane Engineering & Technology Co., Ltd., China. De-ionized water from a Millipore ultrapure water system was used in all the experiments.

2.2. Fabrication of PDMS–SiO_2 nanocomposite membranes

Tween 80/Span 80 (weight ratio = 1:1) mixed surfactant, TEOS, as well as PDMS oligomer were dissolved in *n*-heptane at room temperature to make a homogeneous solution (the mass ratio of TEOS/PDMS oligomers was 0.10, 0.15 and 0.20). Protamine was suspended with a concentration of 10 mg/mL in a 30 mM, pH 7.0 Tris–HCl buffer solution. And then required amount of the protamine aqueous solution was dropwise added into the as-prepared oil solution under vigorous mechanical stirring (water/surfactant mass ratio was from 0.75 to 0.45). After stirring for 30 min, small amount of dibutyltin dilaurate that served as catalyst for the crosslinking reaction of PDMS and TEOS was added. Then, the resulting solution was cast on polysulfone substrate to form thin films. After drying at room temperature for 24 h, the nanocomposite membranes were thermally annealed at 80 °C for 2 h to terminate cross-linking and evaporate the residual solvent. PDMS was able to form thin and robust membrane in our experimental condition. All membrane samples were stored in dust free and dry environment before being used in the separation experiments.

2.3. Characterizations

The morphology of the cross section of the nanocomposite membranes were observed with a field emission scanning electron microscope (FESEM, Nanosem 430). Fluorescence microscope images were taken using an Olympus BX41 microscope. Brunauer–Emmett–Teller (BET) surface area and size distribution measurement of the silica were performed using an ASAP 2020 BET system. Solid-state ^{29}Si-nuclear magnetic resonance (NMR) was recorded on Infinity Plus-400 MHz operating at a frequency of 79.4 MHz for the ^{29}Si nucleus and using the magic angle spinning technique. X-ray diffraction (XRD) patterns were recorded using a Rigaku D/max 2500 v/pc X-ray diffractometer. The thermogravimetry analysis (TGA) was measured by TGA-50, Shimdzu thermogravimetric analyzer with a nitrogen flow of 25 mL min^{-1}. Dynamic mechanical analysis (DMA) were performed using a Q800 (TA Instruments, USA) with a liquid nitrogen cooler. Positron annihilation lifetime spectra (PALS) experiment was conducted by using an ORTEC fast–fast coincidence system (resolution 202 ps) at room temperature. The integral statistics for each spectrum was more than 1×10^7 coincidences. The spectrum was analyzed via "The Maximum Entropy for Life Time analysis" (*MELT*) program [25], which used linear filtering and the method of maximum entropy. The entropy weight range was 5×10^{-9}. The cut-off value was 5×10^{-3}.

2.4. Pervaporative desulfurization experiments

The desulfurization performance of the PDMS–SiO_2 nanocomposite membranes was evaluated using thiophene/*n*-octane mixtures as the model gasoline. The sulfur mass fraction was 500 ppm. The scheme of the pervaporation set-up and the configurations of the membrane module were reported in our previous study [26]. The membrane module was a flat sheet and the effective area of the membrane was 2.56×10^{-3} m^2. The feed solution was pumped into the membrane cell with the flow rate 40 L/h. The temperature of feed flow was controlled at 30 °C. The pressure in the downstream side was maintained at <1.0 kPa using a vacuum pump, and the permeate vapor was collected in liquid nitrogen traps. It should be noted that the testing was performed after steady state conditions have been achieved. The permeation flux (J, kg/(m^2 h)) of the membrane was defined as:

$$J = \frac{Q}{A \times t} \quad (1)$$

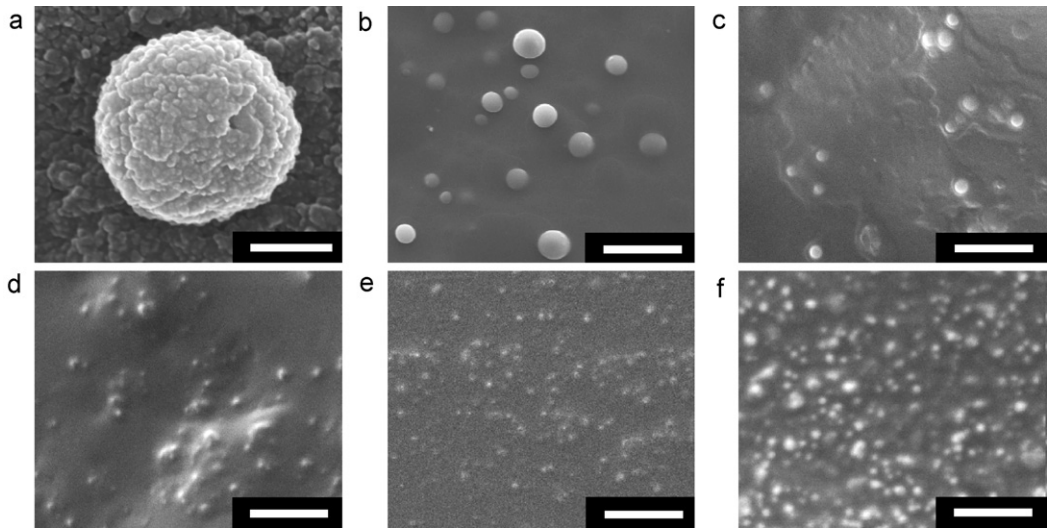

Fig. 1. SEM images (a) surface view of spherical silica particles (R = 0.45). (b and c) Cross-section view of nanocomposite membranes with different spherical silica particle sizes (R = 0.70, 0.58 and 0.45 respectively). (d–f) Cross-section view of nanocomposite membranes with different spherical silica particle mass fractions (6.98%, 10.68% and 14.88% respectively). The scale bars shown in a–f are 2 μm.

where Q (kg) was the total amount of the permeate collected during the experimental period (t, h), and A (m^2) was the effective membrane area. Normalized permeation rate was defined as:

$$NPR = \frac{Q \times \delta}{t \times A} \quad (2)$$

where δ was the membrane thickness. The normalized permeation rate was defined to eliminate the influence of membrane thickness on the permeability.

The feed and permeate compositions were analyzed by gas chromatography (GC, Agilent 6890, Agilent Technologies Co., Ltd.) equipped with a 50 m long PONA capillary column (Dalian institute of chemical physics, Chinese academy of sciences, Dalian, China) and a flame ionization detector (FID, Agilent Co.). The temperatures for injector, detector and oven were set at 200 °C, 250 °C and 80 °C, respectively. The selectivity of the membrane, expressed by the enrichment factor of thiophene (β), was defined as:

$$\beta = \frac{\omega^P}{\omega^F} \quad (3)$$

where ω^F and ω^P referred to the weight fractions of thiophene in the feed and the permeate, respectively.

3. Results and discussion

3.1. Preparation and characterization of the PDMS–SiO_2 nanocomposite membranes

Protamine, as a potent inducer to catalyze and template silica precipitation *in vitro* was selected as silica-precipitating inducer and dissolved in a Tris–HCl solution (pH ≈ 7.0) [27–29]. PDMS oligomers were dissolved in alkane with TEOS. Reverse emulsion solution was formed by blending the above two solutions with Tween 80/Span 80 mixed surfactant under vigorous mechanical stirring. It should be noted that TEOS coincidently served as both silica precursor and crosslinking agent for PDMS in our formulation. "Protamine aqueous solution-Tween/Span" combination with a PDMS host-polymer matrix provided well-defined hierarchical structures with uniform-sized spherical silica particles embedded homogeneously within the PDMS matrix. As shown in Fig. 1 (b–f), the SEM observations revealed that the size and mass fraction of the spherical silica particles could be modulated by simply changing the R (water/surfactant mass ratio) value and the inorganic precursor amount. Therefore, two points deserve further explorations herein. The first point related to tailoring the particle sizes. Reverse emulsions were dynamic systems where the surfactant geometry and affinity, solvent dielectric constant, water/surfactant ratio, and the coalescence/aggregation probability of the reverse emulsion droplets governed the shape and size of the reverse emulsion domains, as well as the phase stability [30–32]. When R decreased from 0.75 to 0.45, the interfacial tension between the non-polar and polar phase were further reduced and thus the sizes of the reverse emulsion were decreased. Confined within the reverse emulsion microspace, the resultant particle sizes were correspondingly reduced from ca. 1 μm to 200 nm. The second point dealt with tailoring the mass fraction of inorganic component within the polymer bulk. Inorganic precursor and protamine met at the w/o interface of the droplets, and then the precursor underwent hydrolysis and condensation reactions that resulted in the formation of monodisperse spherical particles of silica. The hydrolysis reaction produced silanol groups, followed by co-precipitation with protamine through electrostatic interactions [28]. A typical overall reaction could be written as:

$$Si(OR)_4 + 2H_2O \rightarrow SiO_2 + 4ROH \quad (4)$$

It was thus feasible to tune the silica mass fraction by increasing the TEOS with fixed R and protamine concentration, as shown in Fig. 1(d–f). As testified by TGA (Fig. 2), nanocomposite membranes containing silica particles were clearly observed up to silica/polymer mass fraction of 14.88%. The PDMS control membrane and three nanocomposite membranes containing 6.98%, 10.68% and 14.88% were designated as P1, P2, P3 and P4 in the subsequent discussion. As shown in Fig. 3, the PDMS control membrane (P1) was in the amorphous state. A previous literature reported that silica particles mediated by protamine macromolecules was mainly in amorphous state. The amorphous silica displayed characteristic XRD peak at $2\theta \approx 23^\circ$ [28]. The spectra showed that the intensities of amorphous silica peak at 23° were notably enhanced with increasing silica mass fraction, indicating the higher weight fraction of SiO_2 in the P2–P4 nanocomposite membranes.

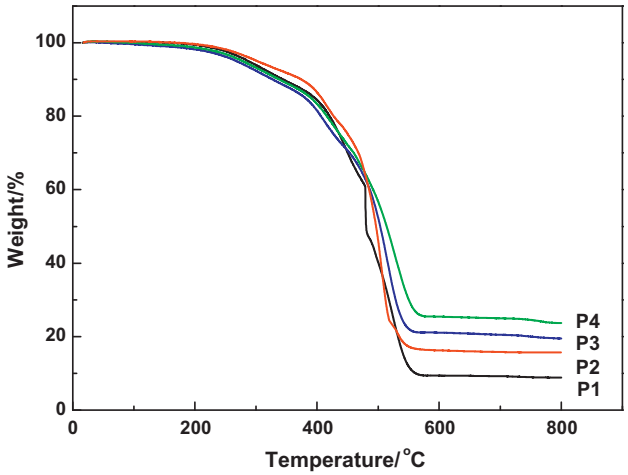

Fig. 2. XRD patterns of PDMS control membrane (P1) and PDMS–SiO_2 nanocomposite membranes (P2–P4).

3.2. Biomimetic mineralization mechanisms in reverse microemulsion

Further studies were necessary for elucidating the role of biomacromolecules during the biomimetic mineralization process. The mesoporosity of the silica particles before/after calcination (600 °C) were evaluated by N_2 adsorption–desorption measurements. In both cases, N_2 adsorption data featured type-II isotherms (Fig. 4). The BET surface area of the calcinated silica and uncalcinated silica was 551.5 $m^2\,g^{-1}$ and 8.7 $m^2\,g^{-1}$. The mesopore diameter of the calcinated sample was 3.0 nm by Barrett–Joyner–Halenda (BJH) analysis, reflecting the template effect of protamine molecules [28]. Fig. 5a showed the fluorescence microscope images of the spherical silica particles catalyzed by fluorescein isothiocyanate (FITC)-labeled protamine in reverse emulsion. The uniformly dispersed green fluorescence demonstrated the homogeneous distribution of the protamine within the silica matrix. In the case of the macromolecule inducers, "Hydrolysis-Convection-Condensation" model was used to account for the silica synthesis in reverse microemulsion, as shown in Fig. 6. TEOS, initially dissolved in the oil phase, penetrated slowly the oil–water interface created by the surfactants. Hydrolysis of TEOS instantly took place once contacting macromolecule inducers in the water phase. As Morse and coworkers [33] described, hydrogen bonding between the hydroxyl side chain of serine and the imidazole side chain of histidine (a specific serine–histidine pair in silicatein) increased the nucleophilicity of the serine oxygen. An attack on the Si atom of the TEOS was facilitated to form a transitory Si–O bond with the protein to initiate hydrolysis of the TEOS at neutral pH. Therefore, it was plausible to assume that protamine could form a similar nucleophilic zone and thus facilitated the hydrolysis of the TEOS. Protamine were cationic proteins with high isoelectric point, the hydrolyzed TEOS anionic molecules (pI of monomeric silicic acid was about 4 [34]) could then form silica/protein nanocomposite at the water–oil interface, leading to the sudden decrease of protein concentration. The proteins in the bulk of water phase subsequently diffused to the water–oil interface, while the silica/protein nanocomposite diffused into the bulk of water phase by convection. Numerous silica/protein nanocomposite subparticles underwent irreversible condensation of adjacent surface hydroxyl groups to form nanocomposite particles till the hydrolyzed TEOS was exhausted. The macromolecule inducers were removed by calcination, leaving uniform mesopores. The templating effect of the macromolecule inducers could be thus validated.

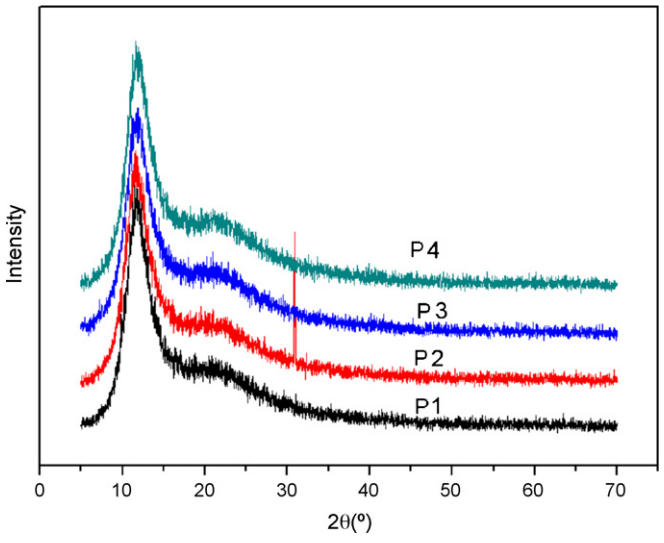

Fig. 3. TGA curve of PDMS control and PDMS–SiO_2 nanocomposite membranes.

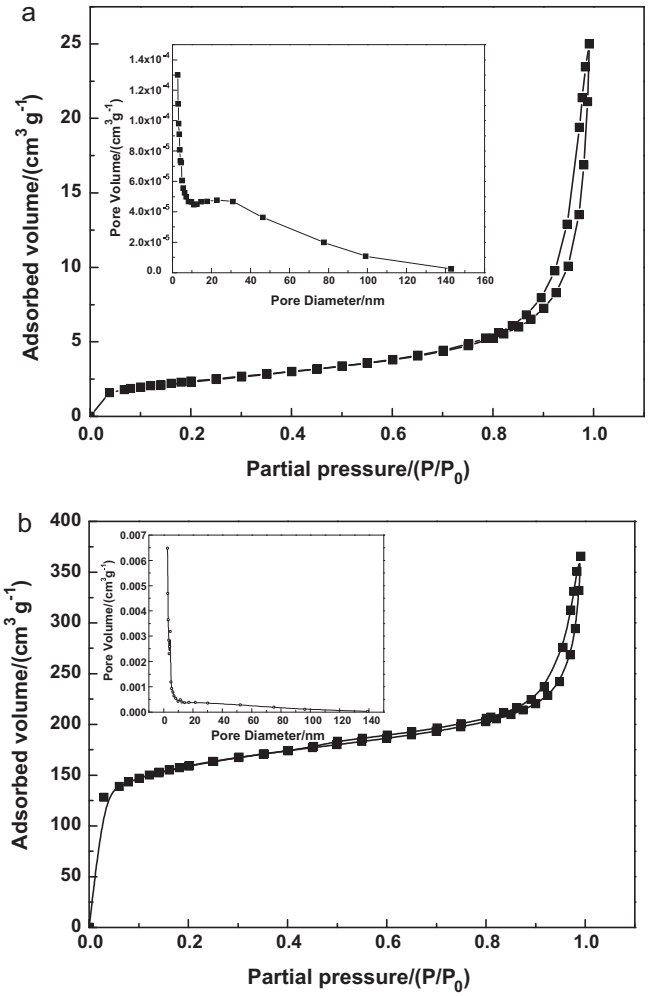

Fig. 4. Nitrogen adsorption isotherm and pore size distribution of (a) uncalcinated and (b) calcinated particles.

The chemical structure of the as-formed silica at the atomic scale was characterized by ^{29}Si-NMR and shown in Fig. 5b. Statistically acceptable spectral deconvolution showed the samples were composed of ca. 6.9% Q_2, 14.1% Q_3 and 79.0% Q_4 Si species

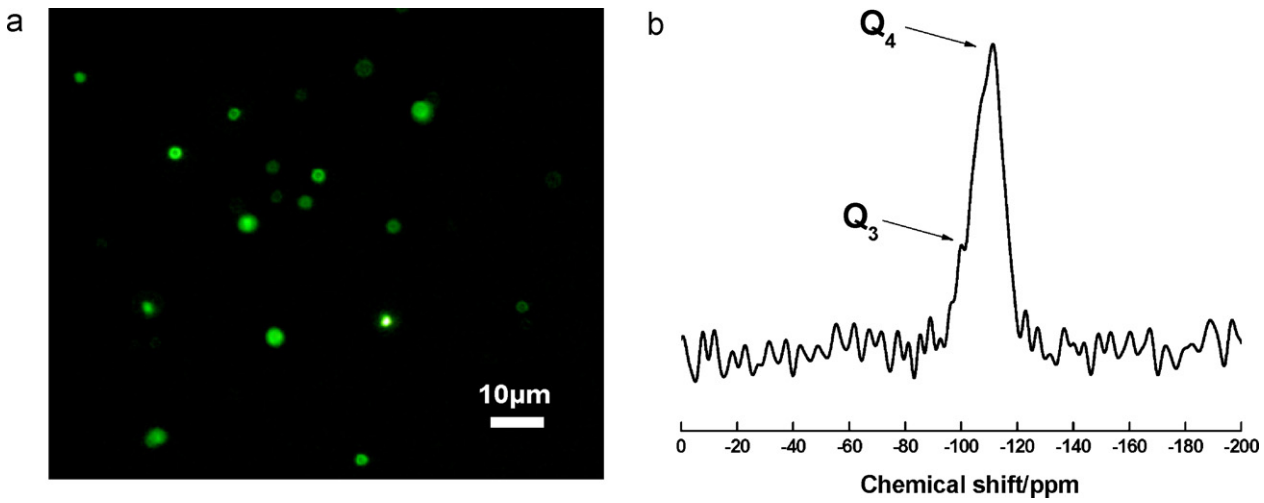

Fig. 5. (a) Fluorescence microscope images of the spherical silica particles catalyzed by FITC-labeled protamine in reverse emulsion. (b) ^{29}Si NMR of the spherical silica particles.

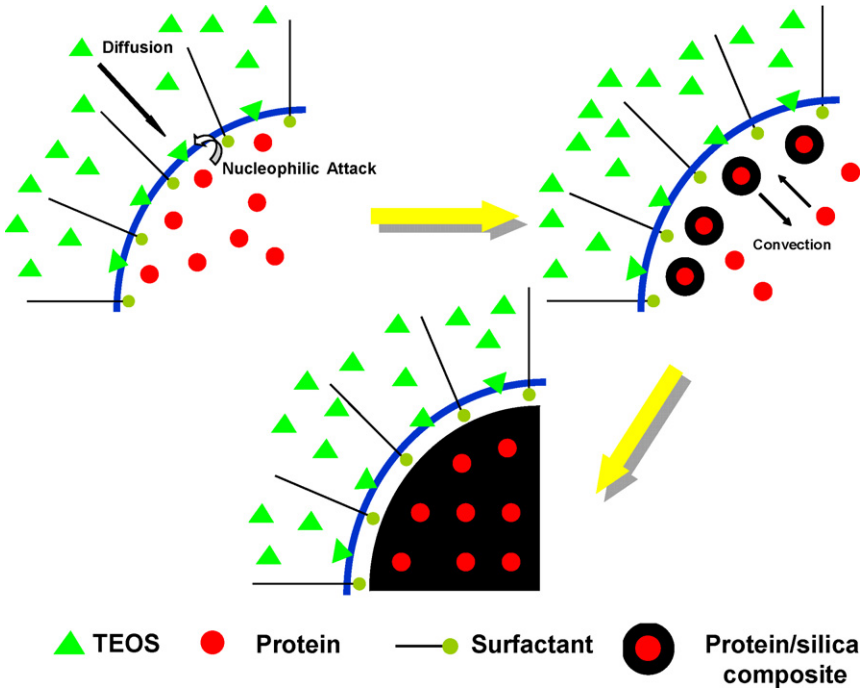

Fig. 6. The formation mechanism of silica mediated by macromolecule inducer in reverse microemulsion.

(where Q_n represented the resonance of a silicon atom bonded to n 'bridging oxygen'). The average Q_4 chemical shift $\delta \approx -110$ p.p.m. corresponded to an average Si–O–Si bond angle (φ) of about 147° according to the Eq. (4) [35]:

$$(\delta)(\text{p.p.m.}) = -0.59(\varphi) - 23.21 \quad (5)$$

The high proportion of Q_3 and Q_4 up to 93.1% demonstrated that well-condensed silica was generated under the catalysis of protamine.

3.3. Free volume and mechanical properties of the PDMS–SiO_2 nanocomposite membranes

Free-volume property could be regarded as one of the most important properties of the nanocomposite membranes. Positron beams was used to directly quantify the amount, size and size distribution of vacancy-type free-volume in the nanocomposite membranes. The results of free volume pore radius and fractional free volume (*FFV*) were summarized in Table 1 and Fig. 7. Fig. 7a showed the positron annihilation lifetime spectra in PDMS control membrane and PDMS–SiO_2 nanocomposite membranes with different SiO_2 content (corresponding to the membranes in Fig. 1(d–f)). The higher the content of SiO_2 in PDMS, the slower

Table 1
Free volume parameters of the PDMS control and PDMS–SiO_2 nanocomposite membranes.

SiO_2 content [wt%]	r_3 [nm]	I_3 [%]	*FFV*
0.00	0.346	14.0	0.0243
6.98	0.346	14.5	0.0251
10.68	0.346	17.8	0.0309
14.88	0.346	21.5	0.0373

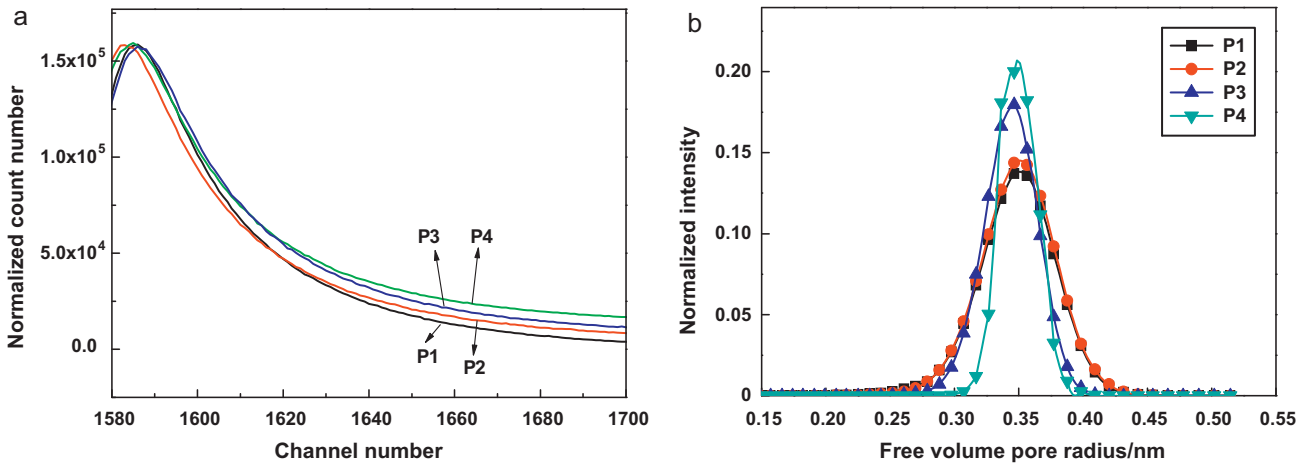

Fig. 7. (a) Positron annihilation lifetime spectra and (b) Distribution of free volume pore radius of PDMS control and PDMS–SiO_2 nanocomposite membranes with different silica mass fraction.

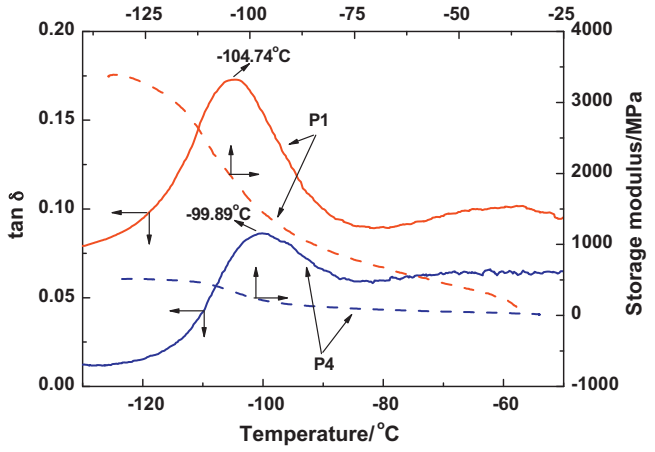

Fig. 8. DMA curves including storage modulus and tan δ as a function of temperature for PDMS control and PDMS–SiO_2 nanocomposite membranes.

the positron lifetime spectral decayed, which indicated that the fractional free volume of the nanocomposite membranes became larger. Fig. 7b represented the free volume pore size distribution of PDMS control membrane and PDMS–SiO_2 nanocomposite membranes, both calculated using *MELT* program. The incorporation of SiO_2 considerably narrowed the free volume pore radius distribution and increased the *FFV* of the nanocomposite membranes, which was most possibly ascribed to the disruption of SiO_2 toward the polymer chain packing. It was well known that PDMS was featured by its high *FFV*, because its Si–O bond length was 1.64 Å, longer than that for the C–C bond (1.53 Å). Also, the Si–O–Si bond angle was approximately 143°, larger than the usual tetrahedral value (ca. 110°) [36]. Undoubtedly, rubbery PDMS composed of nanovoids with a more uniform diameter, as demonstrated in the current study, has great potential in the precise size exclusive separation of molecules. The DMA of the PDMS control and nanocomposite membranes containing 14.88% silica depicted the curves of the samples over a wide range of temperature. As shown in Fig. 8, the storage modulus of the specimens increased with

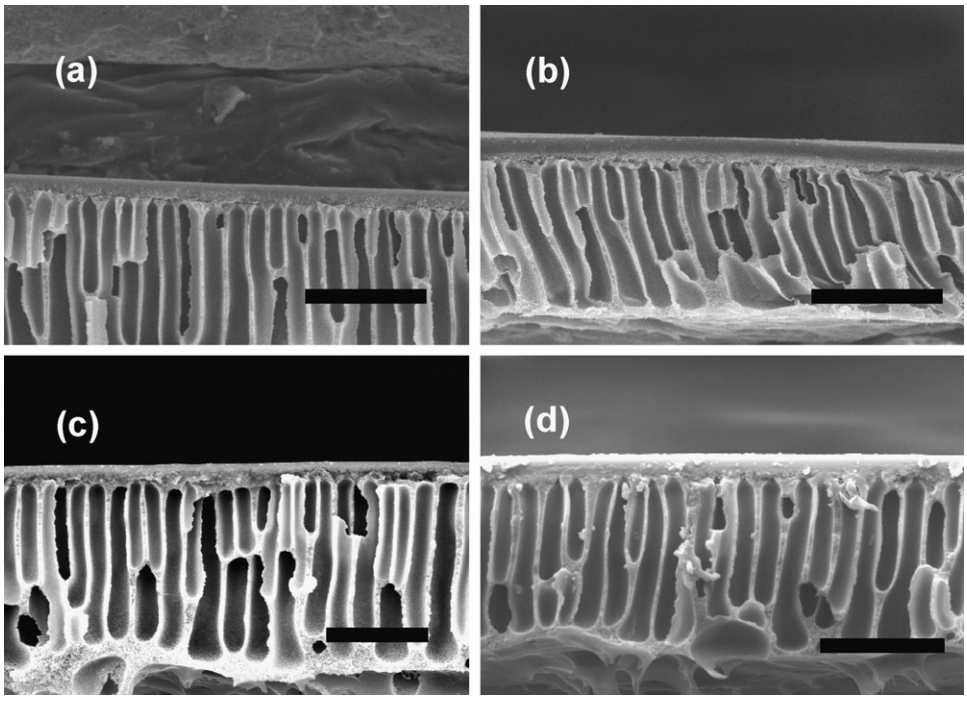

Fig. 9. SEM images of the composite membranes (a) P1, (b) P2, (c) P3, and (d) P4. Scale bars: 50 μm.

higher content of SiO_2, revealing that the interactions between PDMS segmental chains and SiO_2 allowed a fine load transfer and endowed improved mechanical strengths. Due to the increase of the fractional free volume, the glass transition temperature of the nanocomposite membranes appeared to slightly decrease.

3.4. Separation property of the PDMS–SiO_2 nanocomposite membranes

In the present study, the separation performance (binary mixture: *n*-octane/thiophene) of the PDMS–SiO_2 nanocomposite membranes was investigated. Fig. 9 showed the complete cross-section of the composite membranes (P1–P4). The thickness of the active layer was measure to be 10–12 μm. As shown in Fig. 10a, the normalized permeation rate of PDMS control membrane was 6.61×10^{-5} kgm/m^2 h, whereas the normalized permeation rate of the nanocomposite membrane containing 14.88 wt% silica was increased to 10.76×10^{-5} kg m/m^2 h; the enrichment factor of thiophene was only slightly decreased from 5.82 to 4.83. Compared with other membrane materials [7], the current membrane exhibited rather good overall separation performance. The separation between thiophene and *n*-octane could be described by solution-diffusion mechanism. During pervaporation process, thiophene was more permeating component through the membrane. The PDMS control membrane exhibited negative sorption selectivity toward thiophene [37]. Compared with thiophene (20.0 MPa$^{0.5}$), the solubility parameter of PDMS (14.9 MPa$^{0.5}$) was much closer to that of *n*-octane (15.0 MPa$^{0.5}$), which governed *n*-octane to preferentially dissolve in PDMS matrix. However, the diffusion coefficient of thiophene was greater than that of *n*-octane due to the smaller molecular size of thiophene (0.53 nm) compared with *n*-octane (0.63 nm). Therefore, the preferential permeation of thiophene in the PDMS control membrane or PDMS–SiO_2 nanocomposite membranes should be ascribed to the diffusion process rather than solution process. As proved by PALS, the incorporation of silica into the PDMS matrix significantly enlarged the *FFV*. Consequently, the nanocomposite membranes could offer more diffusion paths for those small penetrants. Because the free volume cavity size kept almost unchanged, the selectivity of the membrane was not sharply decreased.

It should be noted that the separation enrichment factor of 4–5 meant the permeate stream contained of about 2000–2500 ppm thiophene from starting feed gasoline mixture containing 500 ppm thiophene. If it was expected to obtain product oil with thiophene concentration of 50 ppm or less from the gasoline–thiophene feed, actually, we could make flexible adjustments of membrane modules according to the different requirements of the thiophene concentration in the product oil. For example, lower target thiophene concentration might require more membrane modules that were connected in series or larger membrane area in a single membrane module. In addition, it should be mentioned that the coupling of pervaporation membrane process and hydrodesulfurization might be more feasible in some situations where pervaporation acted as the pretreatment step prior to hydrodesulfurization.

The effects of different operation conditions such as separation temperatures and feed flow rate on the separation performance of the membrane were investigated. Fig. 10b presented the pervaporation performance of the P2 membrane at temperatures ranging from 30 °C to 60 °C. An increase in operating temperature enhanced the membrane permeation flux, however, reduced the enrichment factor. On one hand, at higher temperature, the polymer chains were more flexible, which might generate larger available free volume of the membrane for diffusion. Hence, total flux increased with feed temperature. On the other hand, because of the more serious swelling of membrane, the selectivity decreased. The

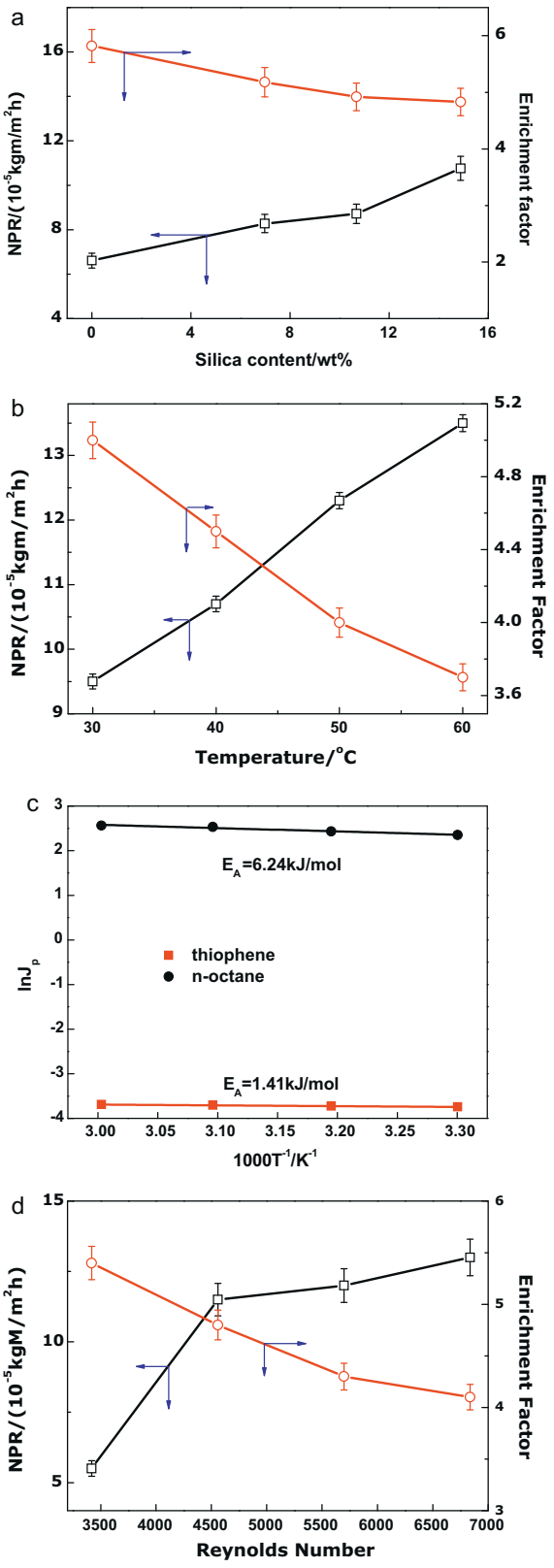

Fig. 10. (a) Effect of silica mass fraction on the separation performance of the PDMS–SiO_2 nanocomposite membranes (feed temperature: 30 °C, flow rate: 40 L/h, and concentration: 500 ppm sulfur); (b) effect of operating temperature on the pervaporation performance of PDMS–SiO_2 nanocomposite membranes (flow rate: 40 L/h, concentration: 500 ppm sulfur); (c) Arrhenius plots of pervaporation flux for the separation of thiophene/n-octane mixture by the PDMS–SiO_2 nanocomposite membranes; (d) effect of Reynolds number on the pervaporation performance of PDMS–SiO_2 nanocomposite membranes (feed temperature: 30 °C, concentration: 500 ppm sulfur).

temperature dependence of the permeation flux could be expressed by Arrhenius relationship:

$$J_P = A_P \exp\left(\frac{-E_A}{RT}\right) \quad (6)$$

where J_P was the permeation flux, A_P was a constant, E_P represented the apparent activation energy for permeation, and T was the absolute temperature. As shown in Fig. 10c, the fitted apparent activation energies from the slope were $E_{octane} = 6.24\ kJ\ mol^{-1}$, $E_{thiophene} = 1.41\ kJ\ mol^{-1}$ at 500 ppm feed sulfur concentration, which indicated that the transport of octane molecules through the membrane was more sensitive to the operating temperature.

The effect of feed flow was presented using the Reynolds number. The calculation process could be referred to previous literature [37]. As shown in Fig. 10d, the total flux increased at higher Reynolds number. With the increase of Reynolds number, the thickness of boundary layer was decreased. Therefore, mass transfer resistance in boundary layer at the upstream side of membrane decreased, which led to the increase of permeation flux. Enrichment factor decreased from 5.4 to 4.1 with Reynolds number increasing, possibly due to the weakened permeation difference between thiophene and *n*-octane.

4. Conclusions

This study tentatively proposed a novel and facile method of one-step fabrication of PDMS–SiO_2 nanocomposite membranes. The membranes displayed superior performance for the removal of organosulfur compounds from model FCC gasoline by energy-saving and environment-benign pervaporation process. Through the controlled biomineralization mediated by inorganic-precipitating molecules at w/o interface, the inorganic mineral formed could be homogeneously embedded into polymer bulk matrix, rendering the nanocomposite membranes with tunable free volume properties and enhanced mechanical stability. The as-prepared PDMS membranes exhibited the enrichment factor of 4.83–5.82 with a normalized permeation rate of $6.61–10.76 \times 10^{-5}\ kgm/m^2h$ for 500 ppm sulfur in feed (40 L/h) at 30 °C. It could be conceived that the as-prepared hydrophobic/oleophilic nanocomposite membranes would find a variety of applications for the efficient removal of hazardous materials.

Acknowledgments

We thank the financial support from the National Basic Research Program of China (No. 2009CB623404), Tianjin Natural Science Foundation (No. 10JCZDJC22600), State Key Laboratory of Materials-Oriented Chemical Engineering of Nanjing University of Technology (No. KL09-3), the program for Changjiang Scholars and Innovative Research Team in University (PCSIRT), the Programme of Introducing Talents of Discipline to Universities (No. B06006).

References

[1] F.C. Menz, H.M. Seip, Acid rain in Europe and the United States: an update, Environ. Sci. Policy 7 (2004) 253–265.
[2] Z. Lu, D.G. Streets, Q. Zhang, S. Wang, G.R. Carmichael, Y.F. Cheng, C. Wei, M. Chin, T. Diehl, Q. Tan, Sulfur dioxide emissions in China and sulfur trends in East Asia since 2000, Atmos. Chem. Phys. 10 (2010) 6311–6331.
[3] European Competences Framework (ECF) standardization, Automotive fuels-unleaded petrol-requirements and test methods, 2008.
[4] The California Reformulated Gasoline Regulations Standardization, 2007.
[5] K. Zhang, J. Hu, S. Gao, Y. Liu, X. Huang, X. Bao, Sulfur content of gasoline and diesel fuels in northern China, Energy Policy 38 (2010) 2934–2940.
[6] S. Brunet, D. Mey, G. Perot, C. Bouchy, F. Diehl, On the hydrodesulfurization of FCC gasoline: a review, Appl. Catal. A-Gen. 278 (2005) 143–172.
[7] L.G. Lin, Y.Z. Zhang, Y. Kong, Recent advances in sulfur removal from gasoline by pervaporation, Fuel 88 (2009) 1799.
[8] A. Bansal, H. Yang, C. Li, K. Cho, B.C. Benicewicz, S.K. Kumar, L.S. Schadler, Quantitative equivalence between polymer nanocomposites and thin polymer films, Nat. Mater. 4 (2005) 693–698.
[9] A.M. Mayes, Nanocomposites: softer at the boundary, Nat. Mater. 4 (2005) 651–652.
[10] T.C. Merkel, B.D. Freeman, R.J. Spontak, Z. He, I. Pinnau, P. Meakin, A.J. Hill, Ultrapermeable, reverse-selective nanocomposite membranes, Science 296 (2006) 519–522.
[11] F.B. Peng, L.Y. Lu, H.L. Sun, Y.Q. Wang, J.Q. Liu, Z.Y. Jiang, Hybrid organic–inorganic membrane: solving the tradeoff between permeability and selectivity, Chem. Mater. 17 (2005) 6790–6796.
[12] A.C. Balazs, T. Emrick, T.P. Russell, Nanoparticle polymer composites: where two small worlds meet, Science 314 (2006) 1107–1110.
[13] H.Y. Chen, E. Ruckenstein, Nanoparticle aggregation in the presence of a block copolymer, J. Chem. Phys. 131 (2009) 244904.
[14] E. Brunner, P. Richthammer, H. Ehrlich, S. Paasch, P. Simon, S. Ueberlein, K. van Pée, Chitin-based organic networks: an integral part of cell wall biosilica in the diatom thalassiosira pseudonana, Angew. Chem. Int. Ed. 48 (2009) 9724–9727.
[15] S. Mann, Self-assembly and transformation of hybrid nano-objects and nanostructures under equilibrium and non-equilibrium conditions, Nat. Mater. 8 (2009) 781–792.
[16] J.N. Cha, G.D. Stucky, D.E. Morse, T.J. Deming, Biomimetic synthesis of ordered silica structures mediated by block copolypeptides, Nature 403 (2000) 289–292.
[17] N. Kröger, S. Lorenz, E. Brunner, M. Sumper, Self-assembly of highly phosphorylated silaffins and their function in biosilica morphogenesis, Science 298 (2002) 584–586.
[18] B. Leng, Z. Shao, P.H.H. Bomans, L.J. Brylka, N.A.J.M. Sommerdijk, G. With, W. Ming, Cryogenic electron tomography reveals the template effect of chitosan in biomimetic silicification, Chem. Commun. 46 (2010) 1703–1705.
[19] F, S. Pan, H.P. Jia, Q.L. Cheng, Z.Y. Jiang, Bio-inspired fabrication of composite membranes with ultrathin polymer–silica nanohybrid skin layer, J. Membr. Sci. 362 (2010) 119–126.
[20] F.S. Pan, Q.L. Cheng, H.P. Jia, Z.Y. Jiang, Facile approach to polymer–inorganic nanocomposite membrane through a biomineralization-inspired process, J. Membr. Sci. 357 (2010) 171–177.
[21] T.L. Simpson, B.E. Volcani, Silicon and Siliceous Structures in Biological Systems, Springer-Verlag, New York, 1981.
[22] J.C. Weaver, D.E. Morse, Molecular biology of demosponge axial filaments and their roles in biosilicification, Microsc. Res. Technol. 62 (2003) 356–367.
[23] S. Mann, Molecular recognition in biomineralization, Nature 332 (1988) 119–124.
[24] A.K. Ganguli, A. Ganguly, S. Vaidya, Microemulsion-based synthesis of nanocrystalline materials, Chem. Soc. Rev. 39 (2010) 474–485.
[25] A. Shukla, M. Peter, L. Hoffman, Analysis of positron lifetime spectra using quantified maximum entropy and a general linear filter, Nucl. Instrum. Methods A 335 (1993) 310–317.
[26] C.L. Hu, R.L. Guo, B. Li, X.C. Ma, H. Wu, Z.Y. Jiang, Development of novel mordenite-filled chitosan–poly(acrylic acid) polyelectrolyte complex membranes for pervaporation dehydration of ethylene glycol aqueous solution, J. Membr. Sci. 293 (2007) 142–150.
[27] Y.J. Jiang, D. Yang, L. Zhang, Q.Y. Sun, X.H. Sun, J. Li, Z.Y. Jiang, Preparation of protamine–titania microcapsules through synergy between layer-by-layer assembly and biomimetic mineralization, Adv. Funct. Mater. 19 (2009) 150–156.
[28] Y.F. Zhang, H. Wu, J. Li, L. Li, Y.J. Jiang, Y. Jiang, Z.Y. Jiang, Protamine-templated biomimetic hybrid capsules: efficient and stable carrier for enzyme encapsulation, Chem. Mater. 20 (2008) 1041–1048.
[29] J. Li, Z.Y. Jiang, H. Wu, L. Zhang, L.H. Long, Y.J. Jiang, Constructing inorganic shell onto LBL microcapsule through biomimetic mineralization: a novel and facile method for fabrication of microbioreactors, Soft Matter. 6 (2010) 542–550.
[30] F.J. Arriagada, K. Osseo-Asare, Synthesis of nanosize silica in a nonionic water-in-oil microemulsion: effects of the water/surfactant molar ratio and ammonia concentration, J. Colloid Interface Sci. 211 (1999) 210–220.
[31] K. Osseo-Asare, F.J. Arriagada, Growth kinetics of nanosize silica in a nonionic water-in-oil microemulsion: a reverse micellar pseudophase reaction model, J. Colloid Interface Sci. 218 (1999) 68–76.
[32] F.J. Arriagada, K. Osseo-Asare, Controlled hydrolysis of tetraethoxysilane in a nonionic water-in-oil microemulsion: a statistical model of silica nucleation, Colloids Surf. 154 (1999) 311–326.
[33] J.L. Sumerel, W. Yang, D. Kisailus, J.C. Weaver, J.H. Choi, D.E. Morse, Biocatalytically templated synthesis of titanium dioxide, Chem. Mater. 15 (2003) 4804–4809.
[34] E.R. Pohl, F.D. Osterholtz, Molecular Characterization of Composite Interfaces, Plenum, New York, 1985.
[35] R. Oestrike, High-resolution 23Na, 27Al, and 29Si NMR spectroscopy of framework aluminosilicate glasses, Geochim. Cosmochim. Acta 51 (1987) 2199–2209.
[36] J.E. Mark, Some interesting things about polysiloxanes, Acc. Chem. Res. 37 (2004) 946–953.
[37] B. Li, D. Xu, Z.Y. Jiang, X.F. Zhang, W.P. Liu, X. Dong, Pervaporation performance of PDMS–Ni^{2+}Y zeolite hybrid membranes in the desulfurization of gasoline, J. Membr. Sci. 322 (2008) 293–301.